Super-Resolution Mapping of Enhanced Emission by Collective Plasmonic Resonances

Ruben F. Hamans,[1,2] Matteo Parente,[1,2] Gabriel W. Castellanos,[3] Mohammad Ramezani,[1,3] Jaime Gómez Rivas,[1,3,] Andrea Baldi[1,2,*]*

1. Dutch Institute for Fundamental Energy Research (DIFFER), De Zaale 20, 5612 AJ Eindhoven, The Netherlands

2. Institute for Complex Molecular Systems, Eindhoven University of Technology, P.O. Box 513, 5600 MB Eindhoven, The Netherlands

3. Institute for Photonic Integration, Department of Applied Physics, Eindhoven University of Technology, P.O. Box 513, 5600 MB Eindhoven, The Netherlands

* j.gomez.rivas@tue.nl, a.baldi@differ.nl

KEYWORDS: nanophotonics, light-matter interaction, plasmonics, collective resonances, super-resolution microscopy, single molecule localization

ABSTRACT: Plasmonic particle arrays have remarkable optical properties originating from their collective behavior, which results in resonances with narrow linewidths and enhanced electric fields extending far into the surrounding medium. Such resonances can be exploited for applications in strong light-matter coupling, sensing, light harvesting, non-linear nanophotonics,

lasing, and solid-state lighting. However, since the lattice constants associated with plasmonic particle arrays are of the order of their resonance wavelengths, mapping the interaction between point dipoles and plasmonic particle arrays cannot be done with diffraction-limited methods. Here, we map the enhanced emission of single fluorescent molecules coupled to a plasmonic particle array with ~ 20 nm in-plane resolution by using stochastic super-resolution microscopy. We find that extended lattice resonances have minimal influence on the spontaneous decay rate of an emitter, but instead can be exploited to enhance the outcoupling and directivity of the emission. Our results can guide the rational design of future optical devices based on plasmonic particle arrays.

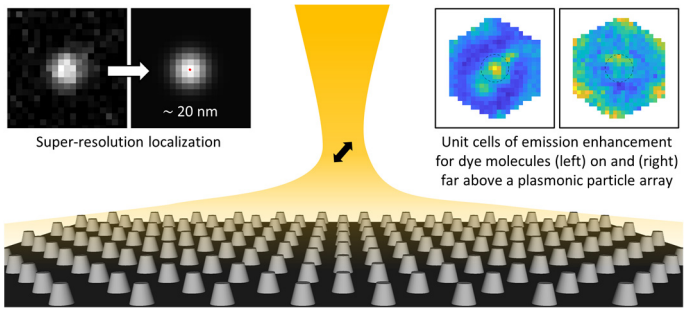

TOC graphic

Localized surface plasmon resonances (LSPRs), arising from the coherent oscillation of free electrons in a metallic nanostructure,[1] can be used to manipulate the absorption and emission of light at the nanoscale.[2-6] Positioning these metallic nanostructures in a periodic array can lead to the formation of collective lattice modes known as surface lattice resonances (SLRs). SLRs are the result of radiative coupling between the LSPRs of individual nanostructures, enhanced by the in-plane orders of diffraction.[7-9] As SLRs are hybrid plasmonic-photonic modes, they are characterized by a linewidth much narrower than that of an LSPR[10-13] and manifest strong electric field enhancements that spatially extend far into the surrounding medium.[14-16] Due to these improved properties and ease of fabrication, SLRs have been investigated thoroughly for applications in sensing,[17] solid-state lighting,[18] lasing,[19-22] and spectroscopy.[23] Additionally, the planar design of structures supporting SLRs and the versatility for integration with other components and materials such as organic fluorophores,[24,25] two-dimensional materials,[26,27] and carbon nanotubes,[28] have attracted significant attention in using arrays of metallic nanoparticles for controlling light-matter interaction at the nanoscale. Hence, improved functionality of optical devices based on SLRs requires an extensive understanding of the interaction between point dipoles and plasmonic particle arrays at the unit cell level. However, the lattice constant of a plasmonic particle array is of the order of its resonance wavelength, resulting in the optical modes having sub-diffraction limit features and being impossible to resolve with conventional optical microscopy.

Here, we use stochastic super-resolution microscopy[29-31] to separately investigate the influence of localized and extended lattice resonances on single molecule emission with sub-diffraction resolution. We combine these measurements with finite-difference time-domain (FDTD) simulations to gain more physical insight into the underlying mechanisms that modify the

emission. We simulate single molecule intensity enhancement as a function of emitter position and disentangle the different contributions by monitoring the Purcell factor, the enhancement in power radiated to the far-field, and the directivity. We find that, despite the extended nature of the SLR, enhanced spontaneous decay rates are only observed in the near-field of the nanoparticles, while the enhanced emission due to the SLR mostly originates from an enhanced directivity.

RESULTS AND DISCUSSION

SAMPLE DESIGN

We design a plasmonic particle array which supports two spectrally separated lattice resonances, both overlapping with the emission of a fluorescent molecule. This sample geometry allows us to separately investigate the influence of different resonances on the emission of single molecules by proper choice of emission filters. The sample is composed of a hexagonal array of aluminum nanostructures with a lattice constant of 450 nm. To obtain a high scattering cross section, each nanostructure is given the shape of a tall truncated cone, with a base diameter of 140 nm, a top diameter of 80 nm, and a height of 150 nm, as shown in Figures 1a,b. The array is fabricated on fused silica using substrate conformal imprint lithography and reactive ion etching, as this technique allows fabrication over large areas with high reproducibility.[32] The extinction spectrum of the array shows two peaks that both overlap with the emission of the caged dye[33] that is used as the fluorescent probe in our study, as shown in Figure 1c (see also Methods and Figure S1). To gain more physical insight into the resonances associated with these peaks, we use FDTD simulations to obtain electric field distributions at the two peaks' wavelengths (see Methods and Figure S2). The resulting electric field distributions demonstrate the distinctive characteristics of

both resonances: the broad resonance centered at 655 nm shows fields that are highly localized to the nanoparticle surface (Figures 1d,e) and we will therefore refer to it as the LSPR. Note that this LSPR is still a hybrid plasmonic-photonic mode, as its dispersion is not fully flat,[34] and therefore does not correspond to the localized surface plasmon resonance of the individual nanoparticles, which is expected to be much broader.[35] The narrow resonance centered at 580 nm, contrary to the LSPR, shows fields that extend far into the surrounding medium (Figures 1f,g) and we will therefore refer to it as the SLR. A detailed description of the origin of these lattice resonances and their electromagnetic properties was already provided in previous work.[34-37] In many other systems based on plasmonic particle arrays, quasiguided modes are also supported,[38] as a high index polymer layer on top of the array can serve as a waveguide. For simplicity, we suppress these modes by using a polymer with a refractive index lower than that of the immersion oil of the microscope objective.

While our microscopy technique allows for a resolution of ~ 20 nm in the x,y-plane of the sample, we also achieve sub-diffraction resolution in the z-direction by confining the dye molecules to a 50 nm thick layer, placed at a height at which it spatially overlaps with the electric field distribution of the LSPR or the SLR.[34]

To investigate the effect of the LSPR on single molecule emission (sample S1 in Figure 1h), we place a 50 nm thick dye-doped polymer layer at the bottom of the nanostructures (z = 0-50 nm), as this position maximizes the overlap with the field in Figure 1d. To investigate the effect of the SLR (sample S2 in Figure 1i), we place a dye layer at z = 250-300 nm, where it overlaps with the extended field in Figure 1f. The Methods section describes the fabrication of these multi-layered polymer structures.

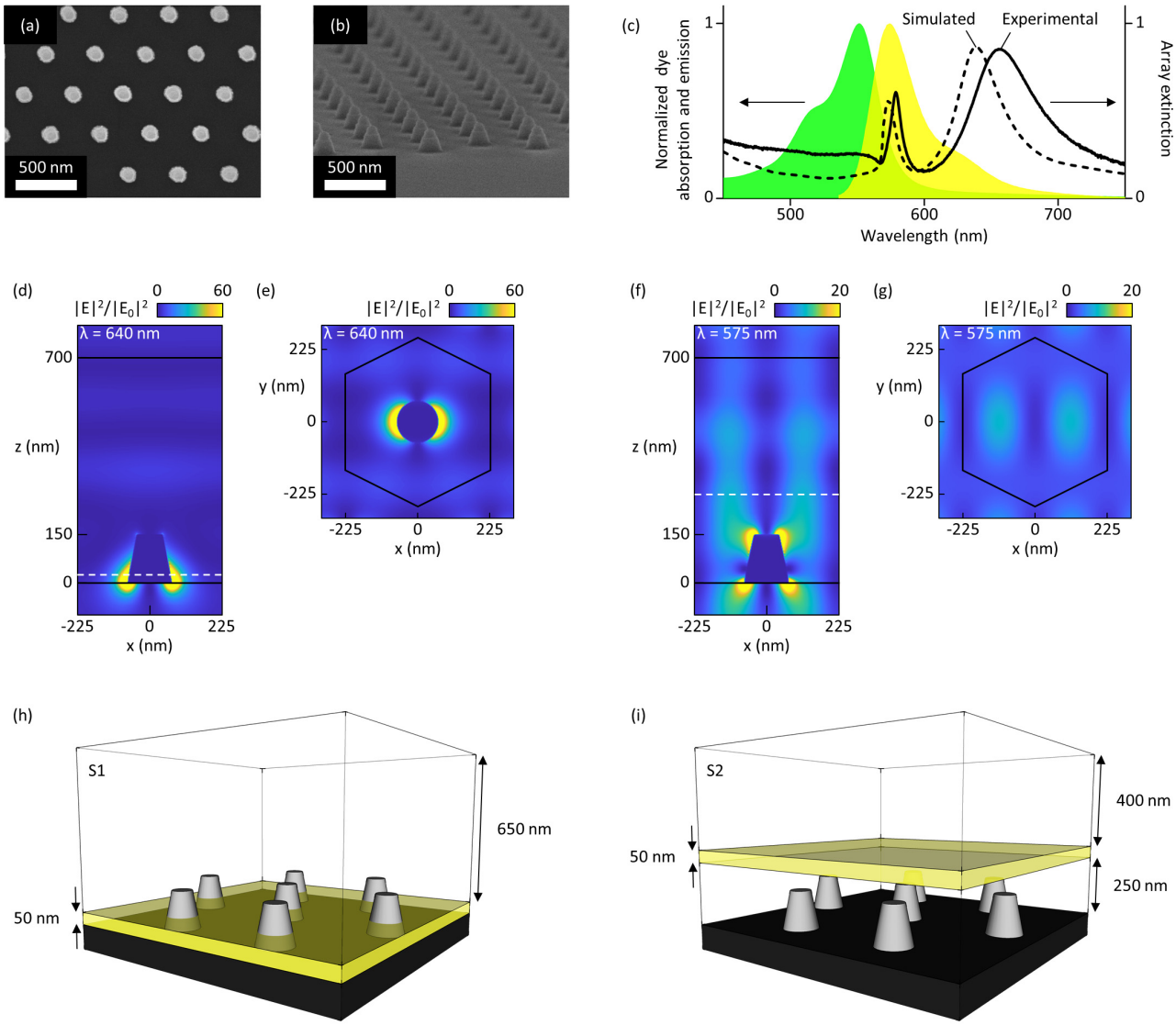

Figure 1. Design and optical properties of the investigated samples. (a) Top view scanning electron microscope (SEM) image of the hexagonal array of aluminum nanostructures. (b) Side view SEM image of the same array. (c) Experimental (solid line) and simulated (dashed line) extinction spectra of the array and normalized absorption (green) and emission (yellow) spectra of the dye in the uncaged state. The absorption and emission spectra were obtained from the dye manufacturer.[33] (d) Simulated (x,z) spatial distribution of the electric field intensity $|E|^2$ normalized to the incident field $|E_0|^2$ at the wavelength corresponding to the

LSPR in the simulated extinction spectrum, λ_{LSPR} = 640 nm. Dielectric interfaces are marked using black lines. (e) Same as (d), but monitored in the (x,y) plane at z = 25 nm, as marked by the dashed white line in (d). The black hexagon marks the unit cell of the array. (f) Same as (d), but for the wavelength corresponding to the SLR, λ_{SLR} = 575 nm. (g) Same as (f), but monitored in the (x,y) plane at z = 275 nm, as marked by the dashed white line in (f). (h) Schematic of sample S1: the transparent box indicates a dye free PMMA layer (n = 1.49) and the yellow box indicates a 50 nm thick PVP layer (n = 1.56) at z = 0-50 nm doped with a caged dye. (i) Schematic of sample S2: same as sample S1, but with the PVP layer containing the dye placed at z = 250-300 nm.

LOCALIZING AND SIMULATING SINGLE EMITTERS COUPLED TO A PLASMONIC PARTICLE ARRAY

The samples are imaged in an inverted optical fluorescence microscope, as illustrated in Figure 2a. At the beginning of each experiment, we first take a transmitted white light image of the array. From this image we localize all nanostructures in the field-of-view of 133 μm by 133 μm by fitting all local maxima in the image to a two-dimensional Gaussian.[39] Due to the high signal-to-noise ratio that can be achieved in the transmitted light image, this fitting procedure results in an estimated localization precision of 7 nm in the x,y-plane of the sample.[39,40] After acquiring the transmitted light image, the sample is illuminated with a 532 nm CW laser to image the fluorescence, as illustrated in Figure 2a. Throughout the experiment we correct for in-plane drift by tracking fluorescent impurities and for out-of-plane drift by using a built-in focus correction system.

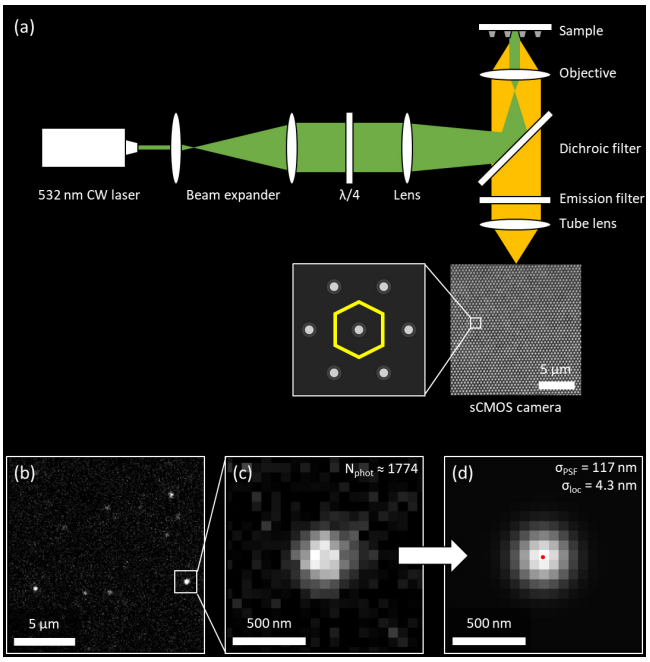

Figure 2. Super-resolution localization of single emitters coupled to a plasmonic particle array. (a) Schematic depiction of the setup: the sample is illuminated at normal incidence with a 532 nm CW laser through the objective of a fluorescence microscope and the emission is imaged on a sCMOS camera. The sCMOS camera image is a cropped transmitted white light image of the plasmonic particle array. The zoom-in drawing schematically illustrates the hexagonal unit cell of the array (yellow hexagon). (b) 250 x 250 pixel cut-out of an example frame of a fluorescence measurement on sample S2 after background subtraction, showing multiple single emitters in the field of view. (c) Zoom of (b), showing the diffraction-limited emission profile of one emitter. The number of photons N_{phot} in each fluorescent event is calculated from the number of photoelectrons per camera count. (d) Two-dimensional Gaussian fit of the emission profile in (c). The fitted molecule position, defined as the center of the 2D Gaussian, is illustrated with the red dot. For this particular event, the width of the fitted Gaussian σ_{PSF} is 117 nm and the estimated localization precision σ_{loc} is 4.3 nm.

The dye-doped polymer layers contain a caged dye,[33] which only becomes fluorescent upon illumination. Using caged dyes allows for a high concentration of dye in the layer, while maintaining a low density of fluorescent events in a single frame, see for example Figure 2b. By keeping the number of fluorescent events per frame low, we can assume that the observed diffraction-limited spots are single molecules, see section 3 of the Supporting Information. We localize these stochastic bursts of single molecule fluorescence by fitting them to a two-dimensional Gaussian, see Figures 2c,d. This fitting procedure results in an estimated localization precision of 15 nm for measurements on sample S1 and 11 nm for measurements on sample S2. As the estimated localization precision scales with $1/\sqrt{N_{phot}}$,[39] where N_{phot} is the number detected of photons, the slightly worse localization precision for sample S1 is due to the worse overlap of the dye emission with the LSPR, see Figure 1c. Since we detect molecules over a large field-of-view, we can average over thousands of nanostructures by redefining the positions of all molecules relative to their nearest nanostructure. This procedure results in all molecule positions falling in a single unit cell, as indicated by the yellow hexagon in Figure 2a. The total estimated localization precision now becomes the sum of the error in localizing the nanostructures and the error in localizing the molecules, resulting in 22 nm for sample S1 and 18 nm for sample S2. A more detailed description of the setup and the image processing can be found in the Methods section and section 4 of the Supporting Information.

For each molecule, we also measure the emission intensity as the total number of detected photons. From all intensities, we can then build a two-dimensional map of the emission intensity as a function of emitter position, where the bin sizes are equal to the estimated localization precision. This map is subsequently normalized with the mean intensity of a molecule detected outside of the array to obtain the experimentally observed enhancement in emission intensity I_{exp}.

The measured changes in intensity are a superposition of modifications in the absorption rate of the dye, their spontaneous decay rate, and the directivity of their emission. To disentangle these contributions, we compare our measurements to FDTD simulations of single electric dipoles coupled to a finite plasmonic particle array (see Methods and section 5 of the Supporting Information). The simulated enhancement in emission intensity I_{sim} is obtained by performing a near-field to far-field transformation on the field monitored in the direction of the objective, in which we neglect all waves propagating at angles that fall outside the numerical aperture of the objective of our microscope (NA = 1.4).

From the three underlying contributions, we neglect modifications in the absorption rate, as the laser wavelength of 532 nm is not resonant with the array, see Figure 1c. We quantify the modification in spontaneous decay rate by monitoring the Purcell factor F_P, which corresponds to the enhancement in the total power radiated by the dipole. As the system investigated here contains aluminum, which is lossy at optical wavelengths, not all photons emitted by the dipole radiate to the far-field. To quantify these losses in the metal, we also monitor the enhancement in total power radiated to the far-field F_{rad}. We define the directivity enhancement D from these simulated values as the ratio between I_{sim} and F_{rad}, as F_{rad} considers the enhancement in all power radiated to the far-field and I_{sim} only the enhancement in the power radiated towards the objective. Since the directivity enhancement D is calculated from I_{sim}, the resulting values for D are also defined for an NA of 1.4.

ENHANCED EMISSION OF SINGLE MOLECULES COUPLED TO A PLASMONIC PARTICLE ARRAY

Since sample S1 contains dye molecules preferentially coupled to the LSPR, we use an emission filter that transmits at the LSPR wavelength, see dashed line in Figure 3a. In this sample we observe strong intensity enhancements of up to ~ 100% for positions corresponding to the center of a nanostructure, as shown in Figure 3b. Although no dye molecules can be present inside the metallic nanostructures, their apparent position in the far-field can be located at the center of the unit cell due to mislocalization effects:[41,42] when a dye molecule is close to a nanostructure, it can excite the LSPR of the nanostructure, which can subsequently radiate to the far-field. This effect results in the fitted position of the molecule being 'pulled' towards the nanostructure. Although the amount of mislocalization decreases with increasing emitter-nanostructure separation, it can still be present for separations of several tens of nanometers.[41] Due to the localized nature of the LSPR, molecules that are close to a nanostructure experience both a strong emission enhancement and strong mislocalization, resulting in the intensity peak at the center of Figure 3b.

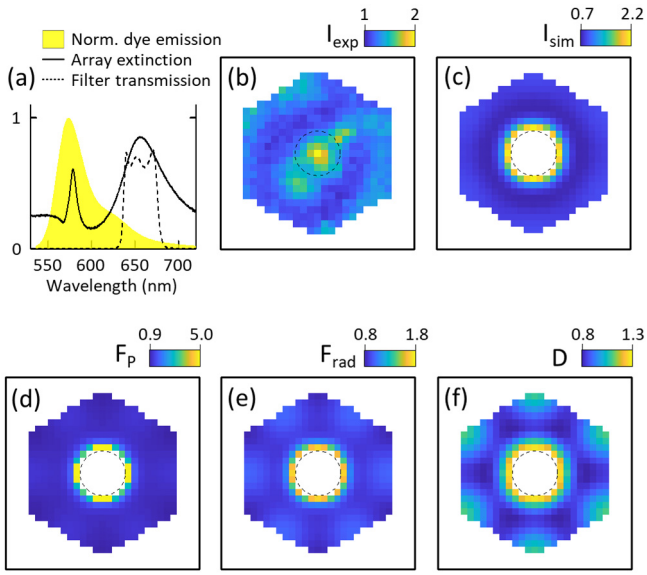

Figure 3. Enhanced emission of single molecules coupled to the LSPR. (a) Normalized dye emission (yellow), array extinction (solid line), and emission filter transmission (dashed line). (b) Two-dimensional histogram of the experimentally observed emission enhancement I_{exp}. Simulated (c) emission enhancement I_{sim}, (d) Purcell factor F_P, (e) enhancement in power radiated to the far-field F_{rad}, and (f) directivity enhancement D. Figure (b) has 22 x 22 nm^2 bins and Figures (c-f) have 20 x 20 nm^2 bins. The dashed lines denote the base of the nanostructure.

The simulated far-field intensity I_{sim} agrees well with the experiment, showing high intensity for dipoles close to a nanostructure, see Figure 3c. The contributions leading to this enhanced emission can be evaluated by comparing Figures 3d-f. Since in this sample some emitters are at nanometer distance from a nanostructure, the change in spontaneous decay rate can become significant.[43] Our simulations confirm this observation, showing Purcell factors up to ~ 5 for small emitter-nanostructure distances, see Figure 3d. Despite such high enhancements, the power radiated to the far-field shows lower peak values, see Figure 3e. This decrease indicates that although the

molecule experiences strong emission enhancement, a substantial fraction is absorbed by the nanostructures.[5] For small emitter-nanostructure distances we also observe enhanced directivity, see Figure 3f. As can be seen when comparing the maximum values in panels e and f of Figure 3, the emission enhancement in this sample is a superposition of a modified spontaneous decay rate and a slight change in directivity. We also perform a control measurement on sample S1 with an emission filter that targets the SLR wavelength and we simulate the emission enhancement at the same wavelength (see Figure S7). Interestingly, we obtain a similar emission enhancement map as in Figure 3b, due to the similar spatial profile of the near-fields at the bottom of the nanoparticles for both the SLR and LSPR (see Figures 1d and 1f).

In sample S2 the emitters preferentially couple to the SLR and we therefore map their emission using a filter that transmits at the SLR wavelength, see dashed line in Figure 4a. In contrast to sample S1, which shows highly localized emission enhancement, we now observe a much more fine structure in the intensity map, see Figure 4b. The highest enhancement is observed at the corners of the unit cell, where the distance to a nanostructure is maximal. The simulations of the far-field intensity I_{sim} accurately reproduce this feature, as shown in Figure 4c. However, the relative weights of the underlying contributions have now shifted substantially. The Purcell factor F_P shows values around unity across the whole unit cell of the array, see Figure 4d, indicating negligible change in the spontaneous decay rate. This observation can be understood from the fact that the Purcell factor scales with the ratio between the quality factor and the mode volume of the resonance.[44] Even though the quality factor is larger for the SLR than for the LSPR, see Figure 1c, the SLR is not confined to the nanostructure surface, see Figure 1f. In other words, due to its extended volume, the SLR has minimal influence on an emitter's spontaneous decay rate. The power radiated to the far-field shows values similar to the Purcell factor, see Figure 4e, indicating

low absorption in the metal due to the large emitter-nanostructure separation in this sample. In contrast to F_P and F_{rad} both showing values around unity, the directivity is enhanced over the whole unit cell of the array due to constructive interference of radiation directed towards the objective, see Figure 4f. From these observations we can conclude that, while SLRs cannot be used to enhance the spontaneous decay rate of emitters, they could be exploited in applications where enhanced directivity over large volumes is required.

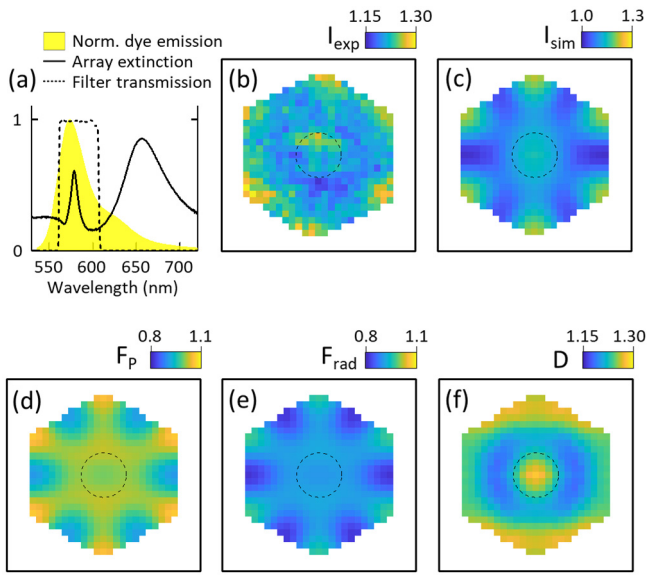

Figure 4. Enhanced emission of single molecules coupled to the SLR. (a) Normalized dye emission (yellow), array extinction (solid line), and emission filter transmission (dashed line). (b) Two-dimensional histogram of the experimentally observed emission enhancement I_{exp}. Simulated (c) emission enhancement I_{sim}, (d) Purcell factor F_P, (e) enhancement in power radiated to the far-field F_{rad}, and (f) directivity enhancement D. Figure (b) has 18 x 18 nm^2 bins and Figures (c-f) have 20 x 20 nm^2 bins. The dashed lines denote the base of the nanostructure.

For sample S2 we also perform control measurements and simulations, now at the LSPR wavelength (see Figure S8). Interestingly, the extended nature of the SLR is now lost, as the enhancement remains limited to molecules in the middle of the unit cell. While both F_P and F_{rad} remain largely unchanged due to the large emitter-nanostructure separation, the directivity enhancement D shows values up to ~ 1.8 for molecules placed right above a nanostructure. Such directivity enhancement is due to light emitted towards the underlying nanoparticle and reflected back into the objective. A similar directivity enhancement is in fact expected for the case of emitters placed above individual aluminum particles (see also SI section 8).

To further investigate the collective nature of the lattice resonances and their influence on single molecule emission, we compare our experiments and simulations on extended arrays to simulations on a single nanostructure. As can be seen in Figures S9 and S10, simulations of dipoles coupled to a single particle can describe most behavior observed in sample S1, both at the SLR and the LSPR wavelength. This result can be understood from the fact that emission enhancement in this sample mostly happens when the dipole is very close to the surface of a nanostructure, where it is not influenced by other nanostructures far away. The emission enhancement we experimentally observe on sample S2, however, is described poorly by simulations on a single particle, see Figures S11 and S12. The emission enhancement at the unit cell corners observed in Figure 4b is not reproduced with a single particle, confirming that this is indeed the result of constructive interference between the scattering from multiple particles. Further discussion on the comparison between the results on the extended array and those on a single particle can be found in section 8 of the Supporting Information.

CONCLUSION

We have demonstrated how stochastic super-resolution microscopy in conjunction with FDTD simulations can be used to study the enhanced emission of single molecules coupled to a plasmonic particle array at the nanometer scale. Combining these methods enables us to disentangle and quantify the different mechanisms leading to the observed emission enhancement. We find that although plasmonic particle arrays have resonances with fields extending far into the surrounding medium, their ability to influence the spontaneous decay rate of an emitter remains limited to small emitter-nanostructure separations. Instead, collective resonances allow us to engineer the radiation pattern of an emitter to obtain directional emission. Our approach of experimentally mapping emission enhancement with sub-diffraction resolution and numerically disentangling the underlying contributions can inform the rational design of optical devices based on plasmonic particle arrays.

METHODS

FABRICATION OF MULTI-LAYERED POLYMER STRUCTURES

Multi-layered polymer structures are fabricated by using combinations of polymers and solvents that do not affect each other. We use polymethylmethacrylate (PMMA, Molecular Weight ~ 350 000 g/mol) with a refractive index of 1.49 dissolved in toluene for the polymer layers without dye and polyvinylpyrrolidone (PVP, Molecular Weight ~ 360 000 g/mol) with a refractive index of 1.56 dissolved in 2-propanol for the layers with dye. For the extinction spectrum shown in Figure 1c, we use a single layer of polyvinylacetate (PVAc, Molecular Weight ~ 500 000 g/mol, dissolved in acetonitrile) with a refractive index of 1.48.

For both samples, the 50 nm thick PVP layer is obtained by spin coating a 1 wt.% solution at 4000 rpm. For sample S1, the 650 nm thick PMMA layer is obtained by spin coating a 6 wt.% solution at 1000 rpm. For sample S2, the bottom 250 nm thick PMMA layer is obtained by spin coating a 4 wt.% solution at 1700 rpm and the top 400 nm thick layer by spin coating a 4 wt.% solution at 600 rpm. The spin coating time is set to 1 minute and the acceleration to 500 rpm/s for all layers.

As can be seen in Figure S1, the resonance wavelengths remain unchanged when changing between polymer layers, due to the small thickness of the PVP layer and the small difference in refractive index between PVAc (used for the extinction spectrum in Figure 1c) and PMMA (used for the super-resolution measurements).

EXTINCTION MEASUREMENTS

To obtain the extinction spectrum in Figure 1c, a fiber coupled laser-based white light source (Energetiq LSDS) is first collimated using a lens. The sample is placed at normal incidence with respect to the collimated beam and the transmitted light is collected with a lens focused on a multimode fiber (Ocean Optics QP600-2-VIS/BX) connected to a spectrometer (Ocean Optics USB2000+). A drop of immersion oil is placed on top of the polymer to mimic the oil-immersion objective that is used for the super-resolution measurements.

The extinction is defined as $1 - T/T_{source}$, where T is the collected spectrum when the beam passes through the array and T_{source} the collected spectrum when the beam passes through an empty part on the same substrate.

FDTD SIMULATIONS OF ELECTRIC FIELD DISTRIBUTIONS

All simulations are performed using 'FDTD Solutions' by Lumerical.[45] The hexagonal periodicity of the array is introduced in the simulations by placing two nanostructures as shown in Figure S2 and by applying periodic boundary conditions. The nanostructures are defined as truncated cones with the dimensions mentioned in the manuscript (150 nm high, 80 nm diameter at the top, and 140 nm diameter at the bottom). The 700 nm thick polymer layer is defined as a lossless dielectric with a refractive index of 1.48 and literature values are used for the complex dielectric function of aluminum and fused silica.[46] The background index is set to that of the immersion oil, 1.52. A plane wave source polarized along the x axis is injected from the top (pointing from the immersion oil to the substrate) and the resulting electric field distribution is monitored in the (x,z) plane and the (x,y) plane.

SUPER-RESOLUTION MEASUREMENTS

Due to the finite absorption at 532 nm of the dye in its caged state and the high absorption at the same wavelength in the uncaged state,[33] one 532 nm CW laser (CNI MGL-FN-532) is used to both uncage and localize the dye. The concentration of dye (300 nM in the solution used for spin coating) and laser power density (6.4 W mm^{-2}) are optimized to give a low enough activation rate (<< 1 per μm^2 in any given frame) while retaining high signal-to-noise ratio.

The setup illustrated in Figure 2a is based around a Zeiss AxioObserver 7 inverted optical fluorescence microscope. The laser beam is expanded using two lenses and its polarization is changed to circular using a $\lambda/4$ plate. The beam is then focused on the back focal plane of the oil-immersion objective (Zeiss Plan-Apochromat 63x/1.4 Oil DIC M27), resulting in illumination normal to the sample.

For the measurement on sample S1 a longpass dichroic filter is used (Chroma AT565DC) with a bandpass emission filter that transmits $\lambda = 650 \pm 20$ nm (Thorlabs FB650-40). For the measurement on sample S2 a custom made dichroic filter is used (Semrock, reflection at $\lambda = 532$ nm and transmission from $\lambda = 550$ nm to $\lambda = 700$ nm) with a bandpass emission filter that transmits $\lambda = 585 \pm 20$ nm (Semrock 585/40 BrightLine).

The signal is imaged on a Hamamatsu ORCA-Flash 4.0 V3 sCMOS camera with 2048 x 2048 pixels and an effective pixel size of 64.5 nm (6.5 μm physical size, used with a 63X magnification objective and an additional 1.6X magnification in the body of the microscope). The integration time is 100 ms and for each experiment 10,000 frames are acquired. The Gaussian fitting is

performed in ThunderSTORM.[40] The image processing is described in more detail in the Supporting Information.

FDTD SIMULATIONS OF SINGLE DIPOLES

The enhanced emission of single molecules is simulated by placing an electric dipole in a finite array of nanostructures. Using periodic boundary conditions is no longer appropriate for these simulations, as this would imply having dipole sources coherently emitting at the same position in each unit cell. The finite array consists of 20 x 20 nanostructures and the z-coordinate of the dipole is in the middle of the dye layer, *i.e.* z = 25 nm for sample S1 and z = 275 nm for sample S2, measured from the substrate.

The Purcell factor F_P is obtained by monitoring the radiated flux out of a box surrounding only the dipole. The enhancement in power radiated to the far-field F_{rad} is obtained with a box surrounding the whole particle array. The transmission through these monitors is normalized to a simulation without nanostructures and averaged over three orthogonal dipole orientations. The resulting values are directly plotted in Figures 3d, 3e, 4d, and 4e. Because of symmetry, simulations are only performed for dipole positions in the first quadrant (positive x and y coordinates) and the results are mirrored to obtain the whole unit cell.

The far-field intensity enhancement I_{sim} is obtained by performing a near-field to far-field transformation on the field monitored above the dipole. All waves propagating at angles higher than the NA of the objective are then filtered out and the remaining waves are projected on an image plane. The resulting far-field emission profile is pixelated to mimic the finite-sized pixels of the camera (see Figures S5 and S6). The far-field intensity I_{sim} plotted in Figures 3c and 4c is defined as the sum over all pixels in an 11 x 11 pixel region around the center (see Figure S6),

normalized to a simulation without nanostructures and averaged over three orthogonal dipole orientations.

The directivity enhancement D plotted in Figures 3f and 4f is defined as I_{sim} divided by F_{rad}, as F_{rad} considers all power radiated to the far-field and I_{sim} only the power radiated towards the objective.

ASSOCIATED CONTENT

Supporting Information. Extinction spectra of all the samples; illustration outlining the FDTD simulations of the electric field distributions; calculation confirming that the observed diffraction-limited spots are single molecules; description of the image processing for the super-resolution measurements; description of how the far-field intensity is simulated; measurements and simulations on sample S1 at the SLR wavelength; measurements and simulations on sample S2 at the LSPR wavelength; simulations on single particles.

AUTHOR INFORMATION

Corresponding Author

*Correspondence to j.gomez.rivas@tue.nl and a.baldi@differ.nl

Author Contributions

R.F.H., M.P., M.R., J.G.R., and A.B. conceived the project; R.F.H., M.P., and M.R. performed the experiments; R.F.H., G.W.C., and M.R. performed the FDTD simulations; J.G.R. and A.B. supervised the project; all authors contributed to writing the paper.

ACKNOWLEDGMENTS

This work was supported by The Netherlands Organisation for Scientific Research (NWO Vidi award 680-47-550 to A.B., NWO Vici award 680-47-628 to J.G.R., the NWO-Signify Industrial Partnership Programme “Nanophotonics for solid-state lighting”, and the NWO Gravitation Programme “Research Centre for Integrated Nanophotonics”). The authors also acknowledge M. Verschuuren for the fabrication of the particle array.

REFERENCES

[1] Bohren, C. F.; Huffman, D. R. Absorption and Scattering of Light by Small Particles, John Wiley & Sons: New York, 2008.

[2] Schuller, J. A.; Barnard, E. S.; Cai, W.; Jun, Y. C.; White, J. S.; Brongersma, M. L. Plasmonics for Extreme Light Concentration and Manipulation. *Nat. Mater.* **2010**, 9, 193-204.

[3] Giannini, V.; Fernández-Domínguez, A. I.; Heck, S. C.; Maier, S. A. Plasmonic Nanoantennas: Fundamentals and Their Use in Controlling the Radiative Properties of Nanoemitters. *Chem. Rev.* **2011**, 111, 3888-3912.

[4] Novotny, L.; van Hulst, N. Antennas for Light. *Nat. Photonics* **2011**, 5, 83-90.

[5] Anger, P.; Bharadwaj, P.; Novotny, L. Enhancement and Quenching of Single-Molecule Fluorescence. *Phys. Rev. Lett.* **2006**, 96, 113002.

[6] Kühn, S.; Håkanson, U.; Rogobete, L.; Sandoghdar, V. Enhancement of Single-Molecule Fluorescence Using a Gold Nanoparticle as an Optical Nanoantenna. *Phys. Rev. Lett.* **2006**, 97, 017402.

[7] Zou, S.; Janel, N.; Schatz, G. C. Silver Nanoparticle Array Structures That Produce Remarkably Narrow Plasmon Lineshapes. *J. Chem. Phys.* **2004**, 120, 10871-10875.

[8] Zou, S.; Schatz, G. C. Narrow Plasmonic/Photonic Extinction and Scattering Line Shapes for One and Two Dimensional Silver Nanoparticle Arrays. *J. Chem. Phys.* **2004**, 121, 12606-12612.

[9] García de Abajo, F. J. Colloquium: Light Scattering by Particle and Hole Arrays. *Rev. Mod. Phys.* **2007**, 79, 1267-1290.

[10] Auguié, B.; Barnes, W. L. Collective Resonances in Gold Nanoparticle Arrays. *Phys. Rev. Lett.* **2008**, 101, 143902.

[11] Kravets, V. G.; Schedin, F.; Grigorenko, A. N. Extremely Narrow Plasmon Resonances Based on Diffraction Coupling of Localized Plasmons in Arrays of Metallic Nanoparticles. *Phys. Rev. Lett.* **2008**, 101, 087403.

[12] Wang, W.; Ramezani, M.; Väkeväinen, A. I.; Törmä, P.; Gómez Rivas, J.; Odom, T. W. The Rich Photonic World of Plasmonic Nanoparticle Arrays. *Mater. Today* **2018**, 21, 303-314.

[13] Kravets, V. G.; Kabashin, A. V.; Barnes, W. L.; Grigorenko, A. N. Plasmonic Surface Lattice Resonances: A Review of Properties and Applications. *Chem. Rev.* **2018**, 118, 5912-5951.

[14] Vecchi, G.; Giannini, V.; Gómez Rivas, J. Shaping the Fluorescent Emission by Lattice Resonances in Plasmonic Crystals of Nanoantennas. *Phys. Rev. Lett.* **2009**, 102, 146807.

[15] Pirruccio, G.; Ramezani, M.; Rodriguez, S. R. K.; Gómez Rivas, J. Coherent Control of the Optical Absorption in a Plasmonic Lattice Coupled to a Luminescent Layer. *Phys. Rev. Lett.* **2016**, 116, 103002.

[16] Chu, C.; Schonbrun, E.; Yang, T.; Crozier, K. B. Experimental Observation of Narrow Surface Plasmon Resonances in Gold Nanoparticle Arrays. *Appl. Phys. Lett.* **2008**, 93, 181108.

[17] Offermans, P.; Schaafsma, M. C.; Rodriguez, S. R. K.; Zhang, Y.; Crego-Calama, M.; Brongersma, S. H.; Gómez Rivas, J. Universal Scaling of the Figure of Merit of Plasmonic Sensors. *ACS Nano* **2011**, 5, 5151-5157.

[18] Lozano, G.; Louwers, D. J.; Rodriguez, S. R. K.; Murai, S.; Jansen, O. T. A.; Verschuuren, M. A.; Gómez Rivas, J. Plasmonics for Solid-State Lighting: Enhanced Excitation and Directional Emission of Highly Efficient Light Sources. *Light: Sci. Appl.* **2013**, 2, e66.

[19] Zhou, W.; Dridi, M.; Suh, J. Y.; Kim, C. H.; Co, D. T.; Wasielewski, M. R.; Schatz, G. C.; Odom, T. W. Lasing Action in Strongly Coupled Plasmonic Nanocavity Arrays. *Nat. Nanotechnol.* **2013**, 8, 506-511.

[20] Ramezani, M.; Halpin, A.; Fernández-Domínguez, A. I.; Feist, J.; Rodriguez, S. R. K.; Garcia-Vidal, F. J.; Gómez Rivas, J. Plasmon-Exciton-Polariton Lasing. *Optica* **2017**, 4, 31-37.

[21] Hakala, T. K.; Rekola, H. T.; Väkeväinen, A. I.; Martikainen, J.-P.; Nečada, M.; Moilanen, A. J.; Törmä, P. Lasing in Dark and Bright Modes of a Finite-Sized Plasmonic Lattice. *Nat. Commun.* **2017**, 8, 13687.

[22] Schokker, A. H.; Koenderink, A. F. Lasing at the Band Edges of Plasmonic Lattices. *Phys. Rev. B* **2014**, 90, 155452.

[23] Adato, R.; Yanik, A. A.; Amsden, J. J.; Kaplan, D. L.; Omenetto, F. G.; Hong, M. K.; Erramilli, S.; Altug, H. Ultra-Sensitive Vibrational Spectroscopy of Protein Monolayers with Plasmonic Nanoantenna Arrays. *Proc. Natl. Acad. Sci. U. S. A.* **2009**, 106, 19227-19232.

[24] Rodriguez, S. R. K.; Gómez Rivas, J. Surface Lattice Resonances Strongly Coupled to Rhodamine 6G Excitons: Tuning the Plasmon-Exciton-Polariton Mass and Composition. *Opt. Express* **2013**, 21, 27411-27421.

[25] Väkeväinen, A. I.; Moerland, R. J.; Rekola, H. T.; Eskelinen, A.-P.; Martikainen, J.-P.; Kim, D.-H.; Törmä, P. Plasmonic Surface Lattice Resonances at the Strong Coupling Regime. *Nano Lett.* **2013**, 14, 1721-1727.

[26] Liu, W.; Lee, B.; Naylor, C. H.; Ee, H.-S.; Park, J.; Johnson, A. T. C.; Agarwal, R. Strong Exciton–Plasmon Coupling in MoS_2 Coupled with Plasmonic Lattice. *Nano Lett.* **2016**, 16, 1262-1269.

[27] Tran, T. T.; Wang, D.; Xu, Z.-Q.; Yang, A.; Toth, M.; Odom, T. W.; Aharonovich, I. Deterministic Coupling of Quantum Emitters in 2D Materials to Plasmonic Nanocavity Arrays. *Nano Lett.* **2017**, 17, 2634-2639.

[28] Zakharko, Y.; Graf, A.; Zaumseil, J. Plasmonic Crystals for Strong Light–Matter Coupling in Carbon Nanotubes. *Nano Lett.* **2016**, 16, 6504-6510.

[29] Betzig, E.; Patterson, G. H.; Sougrat, R.; Lindwasser, O. W.; Olenych, S.; Bonifacino, J. S.; Davidson, M. W.; Lippincott-Schwartz, J.; Hess, H. F. Imaging Intracellular Fluorescent Proteins at Nanometer Resolution. *Science* **2006**, 313, 1642-1645.

[30] Hess, S. T.; Girirajan, T. P. K.; Mason, M. D. Ultra-High Resolution Imaging by Fluorescence Photoactivation Localization Microscopy. *Biophys. J.* **2006**, 91, 4258-4272.

[31] Rust, M. J.; Bates, M.; Zhuang, X. Sub-Diffraction-Limit Imaging by Stochastic Optical Reconstruction Microscopy (STORM). *Nat. Methods* **2006**, 3, 793-795.

[32] Verschuuren, M. A. Substrate Conformal Imprint Lithography for Nanophotonics, Utrecht University: Utrecht, 2010.

[33] Abberior CAGE 552. https://www.abberior.com/jtl-shop/Abberior-CAGE-552 (accessed Feb 28, 2019).

[34] Ramezani, M.; Lozano, G.; Verschuuren, M. A.; Gómez Rivas, J. Modified Emission of Extended Light Emitting Layers by Selective Coupling to Collective Resonances. *Phys. Rev. B* **2016**, 94, 125406.

[35] Lozano, G.; Barten, T.; Grzela, G.; Gómez Rivas, J. Directional Absorption by Phased Arrays of Plasmonic Nanoantennae Probed with Time-Reversed Fourier Microscopy. *New J. Phys.* **2014**, 16, 013040.

[36] Rodriguez, S. R. K.; Bernal Arango, F.; Steinbusch, T. P.; Verschuuren, M. A.; Koenderink, A. F.; Gómez Rivas, J. Breaking the Symmetry of Forward-Backward Light Emission with Localized and Collective Magnetoelectric Resonances in Arrays of Pyramid-Shaped Aluminum Nanoparticles. *Phys. Rev. Lett.* **2014**, 113, 247401.

[37] Yang, A.; Hryn, A. J.; Bourgeois, M. R.; Lee, W.-K.; Hu, J.; Schatz, G. C.; Odom, T. W. Programmable and Reversible Plasmon Mode Engineering. *Proc. Natl. Acad. Sci. U. S. A.* **2016**, 113, 14201-14206.

[38] Rodriguez, S. R. K.; Murai, S.; Verschuuren, M. A.; Gómez Rivas, J. Light-Emitting Waveguide-Plasmon Polaritons. *Phys. Rev. Lett.* **2012**, 109, 166803.

[39] Thompson, R. E.; Larson, D. R.; Webb, W. W. Precise Nanometer Localization Analysis for Individual Fluorescent Probes. *Biophys. J.* **2002**, 82, 2775-2783.

[40] Ovesný, M.; Křížek, P.; Borkovec, J.; Švindrych, Z.; Hagen, G. M. ThunderSTORM: a Comprehensive ImageJ Plug-In for PALM and STORM Data Analysis and Super-Resolution Imaging. *Bioinformatics* **2014**, 30, 2389-2390.

[41] Wertz, E.; Isaacoff, B. P.; Flynn, J. D.; Biteen, J. S. Single-Molecule Super-Resolution Microscopy Reveals How Light Couples to a Plasmonic Nanoantenna on the Nanometer Scale. *Nano Lett.* **2015**, 15, 2662-2670.

[42] Wertz, E.; Isaacoff, B. P.; Biteen, J. S. Wavelength-Dependent Super-Resolution Images of Dye Molecules Coupled to Plasmonic Nanotriangles. *ACS Photonics* **2016**, 3, 1733-1740.

[43] Guo, K.; Verschuuren, M. A.; Koenderink, A. F. Superresolution Imaging of the Local Density of States in Plasmon Lattices. *Optica* **2016**, 3, 289-298.

[44] Purcell, E. M. Spontaneous Emission Probabilities at Radio Frequencies. *Phys. Rev.* **1946**, 69, 681.

[45] Nanophotonic FDTD Simulation Software – Lumerical FDTD Solutions. https://www.lumerical.com/tcad-products/fdtd/ (accessed Feb 28, 2019).

[46] Palik, E. D. Handbook of Optical Constants of Solids, Academic Press: Orlando, 1985.